Acta Geodyn. Geomater., Vol. 21, No. 3 (215), 253–266, 2024
DOI: 10.13168/AGG.2024.0021
journal homepage: https://www.irsm.cas.cz/acta

ORIGINAL PAPER

THEORY OF PRESSURE-TENSION FAILURE AND ITS APPLICABILITY ANALYSIS

Hao LIU [1], Xin JIANG [1] *, Quanming ZHANG [2], Wei LIU [2], Yaguang LONG [2] and Ke ZHAI [2]

[1] *Mining Engineering Research Institue, Shandong University of Science and Technology, Taian 271000, China*
[2] *Xinglongzhuang Coal Mine, Yankuang Energy Group Co.,Ltd., Jining 272004,China*

**Corresponding author's e-mail:* xinjiang2208@163.com

ARTICLE INFO

Article history:
Received 5 May 2024
Accepted 12 September 2024
Available online 30 September 2024

Keywords:
Rock failure characteristics
Failure mode
Pressure-tension strength criterion
Pressure-shear failure

ABSTRACT

The traditional tension-shear failure criterion has proved unable to explain the objective reality of rock tension failure under pressure. It also overestimates the failure strength of rock tension failure under pressure. By combining the hypothesis of a nonuniform rigid body mode with the theory of maximum normal stress, the formation mechanism of rock tension cracks under pressure is described. A new pressure-tensile failure strength criterion capable of giving full description of rock failure strength and failure characteristics under complex stress is proposed. By summarizing related test results, the universality and accuracy of the pressure tension strength criterion are verified. A PT–PS model capable of identifying pressure–tensile failure zones and pressure–shear failure zones is established and compared with the traditional model. The results show that as the traditional model overestimates rock strength under P–T state, when $\lambda \leq 1/3$ or $\lambda \geq 3$, it underestimates the range of the roadway surrounding rock plastic zone. This underestimation will further increase with the increase or decrease of λ. The PT–PS model gives a more realistic picture of roadway surrounding rock failure. Our new model can provide meaningful reference for evaluating the stability and designing the supports of underground works.

1. INTRODUCTION

The traditional tension–shear failure criterion generally relies on the Mohr–Coulomb strength criterion as the basis for identifying surrounding rock shear failure (Denise and Quevedo, 2020; Li et al., 2020; Zang et al., 2020), as shown in Figure 1. Nevertheless, existing studies have demonstrated that the mode of rock failure under tension-compression with less tension (AO section), uniaxial compression or low confining pressure (OB section) is much different from that of pure shear failure; the Mohr–Coulomb cannot give an accurate description of the failure strength of rocks in this interval (AB section).

So far, effective mechanical testing of rocks under tension-compression stresses (AO section) is not realized effectively. According to elastic mechanics, tension-compression stressing can be approximated to tension-shearing. Experimental studies around the failure of rocks under tension-shear stresses have been reported since the mid-20th century. Zhou et al. (2016) conducted full-range tension-shear and pressure-shear testing on rock samples. They discovered that under tension-shear or under pressure-shear stresses with less pressure, tension-shear failure appears on all microfracture surfaces, whereas only pure shear slipping occurs under pressure-shear stresses with high pressure. When conducting full-range tension-shear and pressure-shear testing on rock samples with different lithologies, Li et al. (2014) and Guo et al. (2012) noticed that under tension-shear, tensile failure range of rock intensifies with increasing tensile stress; the tensile stress received by the rock sample is negatively correlated to the shear stress. They also discovered that the slope of rock strength fracture line in the tension-shear section is larger than that in the pressure-shear section. Ramsey (2003) and Ramsey et al. (2004) yielded a complete test data set by realizing the transition from tension fracture to shear fracture, namely, a hybrid fracture, with dog-bone specimens. Rodriguez (2005) presented a detailed analysis on the micro characteristics of fracture surfaces using Ramsey's test results. When simulating rocks under tension-compression with PFC, Huang et al. (2020) and Cen et al. (2020) revealed that with the increase of compressive stress, the inclination angle of rock fracture surfaces will

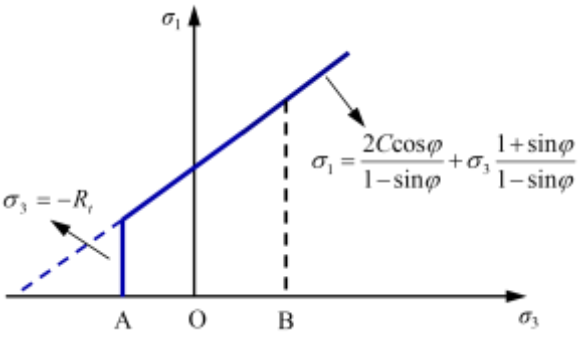

Fig. 1 Traditional tension-shear failure criterion.

Cite this article as: Liu H, Jiang X, Zhang Q, Liu W, Long Y, Zhai K: Theory of pressure-tension failure and its applicability analysis. Acta Geodyn. Geomater., 21, No. 3 (215), 253–266, 2024. DOI: 10.13168/AGG.2024.0021

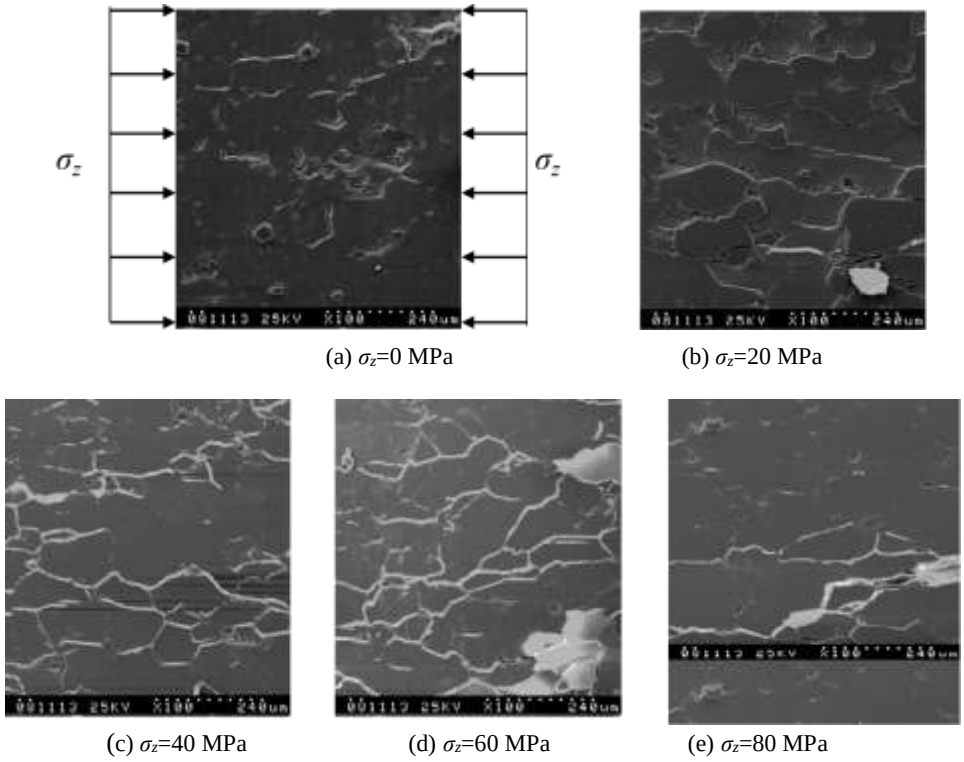

(a) σ_z=0 MPa (b) σ_z=20 MPa

(c) σ_z=40 MPa (d) σ_z=60 MPa (e) σ_z=80 MPa

Fig. 2 Fine structural damages on the rock surface under different axial stresses (Zhu et al., 2013).

gradually increase, too; the fracture mode will also change from tension to tension shear. By loading rock samples under different confining pressures. Some researches Huang et al. (2019), Jiang et al. (2000), Ren (2018), Xie et al. (2021) and Yu et al. (2009) discovered that rocks are subject to splitting failure when under uniaxial or low confining pressures (OB section); with the increase of confining pressure, the failure mode also changes toward shear failure. Through traxial compression loading tests on rocks with different lithologies, research results (Alejano et al., 2017; Arzua. and Alejano, 2013; Arzua et al., 2014; Liu et al., 2014; Wang et al., 2010; Wang et al., 2012; Yang et al., 2006) demonstrated that under low confining pressures, the strength of rock samples is much lower than the triaxial linear regression strength. They suggested that the tension deformation of rocks under low confining pressures makes a difference to their shear strength; with the increase of confining pressure, their strength profile is a broken line with inflections.

The above studies indicate that in the AB section, all rock fracture surfaces display detectable features of tension failure. In that case, the fracture surfaces tend to be opened with no detectable friction between them. Obviously, internal friction angle has nothing to do with rock tension failure, suggesting that the Mohr–Coulomb criterion cannot characterize the failure strength of rocks for tension failure. Also, the theoretical failure strength in the AB section (the high confining pressure linear regression strength based on the Mohr–Coulomb criterion) is much higher than the actual failure strength. When the roadway is excavated or disturbed by dynamic pressure, the surface of the roadway surrounding rock is strongly unloaded. As σ_3 reduces, the maximum principal stress of the surrounding rock will approximate the failure strength of the AB section. This strength criterion that overestimates the failure strength of the AB section will no longer apply to the identification of surrounding rock failure on the roadway surface.

So far, studies around the rock mechanical behavior in the AB section have primarily relied on the summary and analysis of empirical results. Theoretical research on the rock failure mechanism in the AB section has been rare. This paper analyzes the formation mechanism of tension cracks in rocks under pressure, proposes a new pressure-tension (P–T) failure strength criterion, explores the applicability of the new criterion and verifies the accuracy of the criterion. It also builds a model (PT–PS model) capable of identifying pressure-tension failure and pressure-shear failure, compares the differences between the traditional model and the PT–PS model in determining the mode and distribution range of roadway surrounding rock failure.

2. FORMATION OF TENSION CRACKS UNDER PRESSURE

Rock failure is the propagation and interconnection of microfractures (Zhou et al., 2010). Therefore, investigating the causes of tension failure should begin with the microfractures inside rocks. Figure 2 shows the development of rock microfractures recorded by Zhu et al. (2013) in their uniaxial compression experiments on marble.

From Figure 2(a), before the rock sample is loaded, its surface is not homogeneous. Microstructures and defects are found randomly distributed across the rock surface. When the axial stress is 20 MPa, microcracks occur in some defective structures as a result of external load. However, these cracks are limited in number, thickness and length and they propagate in random directions. When the axial stress is 40 MPa, the number of microcracks increases. The earlier cracks lengthen and thicken. Some of them show diffusive microcracks at the tip. When the axial stress is 60 MPa, more new microcracks appear. The earlier cracks lengthen and thicken rapidly along the loading direction. Multiple diffusive cracks are seen at the tip, which intersect with each other to form main cracks. When the axial stress increases to 80 MPa, the main cracks propagate and interconnect quickly along the loading direction, causing the sample to split and fracture. The other cracks are gradually closed and disappeared.

Obviously, the development, propagation, and interconnection of defective structures inside the material constitute the fundamental causes of macro tension failure. In the light of the hypothesis of a nonuniform rigid body mode proposed by Rodionov and Sizov (1982) and Rodionov et al. (1986), it is suggested that at a given deformation rate, a particular size of defective structure can always be found inside the model, where stress will accumulate over time until macro failure occurs. Assuming that there is at least one such defective structure inside the rock where a nonuniform stress field can appear despite any uniform deformation, then according to Maxwell's model for stress relaxation, the evolution of the accumulated stress at the defect can be obtained (Rodionov and Sizov, 1982):

$$\frac{d\Delta\sigma_{qx}}{dt} = KG\varepsilon_p(t) - \omega\frac{\Delta\sigma_{qx}}{s} \tag{1}$$

where:
$\Delta\sigma_{qx}$—accumulated stress at the defect, MPa;
K—stress concentration coefficient at the defect;
$\varepsilon_p(t)$—time-dependent deviatoric strain;
G—rock shear modulus, GPa;
ω—accumulated stress relaxation rate;
s—defect size, mm.

In Eq. 1, $KG\varepsilon_p(t)$ represents the accumulated stress induced by shear strain, which is similar to elastic loading; $\omega\frac{\Delta\sigma_{qx}}{s}$ represents the relaxation or release of the accumulated stress.

Assuming that the rock sample is uniaxially compressed, as shown in Figure 3, and its axial force is loaded at a uniform speed, then its axial force is expressed as (positive for tensile and negative for compressive):

$$\sigma_z(t) = -\sigma_m\frac{t}{T} \tag{2}$$

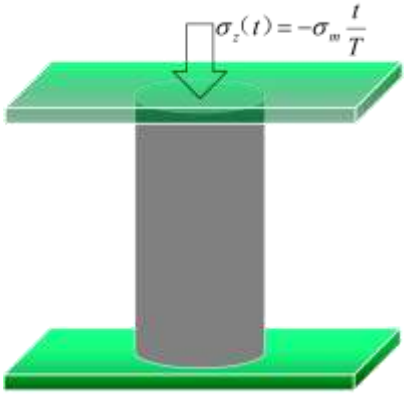

Fig. 3 Schematic diagram of uniaxial loading.

where:
$\sigma_z(t)$—axial pressure, MPa;
t—real loading time, s;
σ_m—target stress;
T—time needed to load to the target stress, s.

Then in the elastic stage, we have:

$$\varepsilon_z(t) = \frac{\sigma_z(t)}{E} = -\frac{\sigma_m t}{ET} \tag{3}$$

$$\varepsilon_x(t) = \varepsilon_y(t) = -v\varepsilon_z(t) = \frac{v\sigma_m t}{ET} \tag{4}$$

Here the deviatoric strain is expressed as:

$$\varepsilon_p(t) = \frac{2\left(\varepsilon_z(t) - \varepsilon_x(t)\right)}{3} \tag{5}$$

Substituting Eqs. (3) and (4) into Eq. (5) yields:

$$\varepsilon_p(t) = -\frac{\sigma_m t}{3GT} \tag{6}$$

where:
$G = \frac{E}{2(1+v)}$.

According to Eq. (1), when the rock is uniaxially compressed in the elastic stage, the stress accumulated at the defect is expressed as:

$$\frac{d\Delta\sigma_z}{dt} = KG\varepsilon_p(t) - \omega\frac{\Delta\sigma_z}{s} \tag{7}$$

And assuming $\Delta\sigma_z$ is Y, $B = \frac{\omega}{s}$, $A = KG\varepsilon_p(t)$, then Eq. (7) can be rewritten as:

$$Y' = A - BY \tag{8}$$

According to the general solutions of ordinary differential equations, we have:

$$Y = Fe^{-Bt} + \frac{A}{B} \tag{9}$$

where:
F is a constant. Substituting Eq. (6) into Eq. (9) yields:

$$Y = Fe^{-\frac{\omega}{s}t} - \frac{Ks\sigma_m}{3\omega T} \tag{10}$$

According to the boundary conditions, before loading, we have t=0, $\Delta\sigma_z$=0, then:

$$\Delta\sigma_z = \frac{Ks\sigma_m}{3\omega T}(e^{-\frac{\omega}{s}t} - 1) \quad (11)$$

Assuming that the accumulated stress relaxation rate(ω) at the defect is very small throughout the loading, then $\left(e^{-\frac{\omega}{s}t} - 1\right) \approx -\frac{\omega}{s}t$. Substituting it into Eq. (11) yields the accumulated stress as:

$$\Delta\sigma_z = -\frac{tK\sigma_m}{3T} = -\frac{K}{3}\sigma_z \quad (t) \quad (12)$$

From Eq. (12), the accumulated stress at the defect increases with increasing axial force of the rock sample. Assuming that the accumulated stress at the defect approximates a shear stress with no volumetric deformation, then:

$$\Delta\sigma_x + \Delta\sigma_y + \Delta\sigma_z = 0 \quad (13)$$

Assuming that the radial accumulated stress at the defect is symmetrical, then:

$$\Delta\sigma_x = \Delta\sigma_y = -0.5\Delta\sigma_z \quad (14)$$

Substituting Eq. (12) into Eq. (14) yields:

$$\Delta\sigma_x = \frac{1}{6}K\sigma_z(t) \quad (15)$$

From Eq. (14), with the increase of axial stress, the tensile stress $\Delta\sigma_x$ induced by the accumulated stress at the defect gradually increases, too, so microcracks begin to propagate. When $\Delta\sigma_x$ reaches the tensile strength, tension failure will occur in the sample. This well explains why longitudinal cracks appear in the rock when axial force is increased, as shown in Eq. (16).

$$\Delta\sigma_x = \frac{1}{6}K\sigma_z(t) = R_t \quad (16)$$

where: R_t—uniaxial tensile strength of the sample, MPa.

Now let us discuss what happens when the rock is triaxially stressed. The rock sample is assumed to be in hydrostatic pressure – σ3, then assumed to Hooke's law, we have:

$$\varepsilon_x = \varepsilon_y = \varepsilon_z = \frac{1-2v}{E}\sigma_3 \quad (17)$$

Now when the rock is axially stressed at a uniform speed, according to Eq. (4) and Eq. (17), the macro average strain of the rock is:

$$\begin{cases} \varepsilon_x(t) = \varepsilon_y(t) = \frac{v\sigma_m t}{ET} - \frac{1-2v}{E}\sigma_3 \\ \varepsilon_z(t) = -\frac{\sigma_m t}{ET} - \frac{1-2v}{E}\sigma_3 \end{cases} \quad (18)$$

Substituting Eq. (18) into Eq. (5) yields the expression of the deviatoric strain as:

$$\varepsilon_p(t) = -\frac{\sigma_m t}{3GT} \quad (19)$$

Eq. (19) yields the same result as Eq. (6). The subsequent solution steps are the same as Eq. (6) through Eq. (15). This way we get the tensile stress induced by the accumulated stress as:

$$\Delta\sigma_x = \frac{1}{6}K\sigma_z(t) \quad (20)$$

In that case the resultant force σ_x received at the defect in the horizontal direction is the combination of hydrostatic pressure -σ_3 with the tensile stress $\Delta\sigma_x$ induced by the accumulated stress. Accordingly, Eq. (20) can be rewritten as:

$$\sigma_x = \frac{1}{6}K\sigma_m\frac{t}{T} - \sigma_3 \quad (21)$$

Obviously, when σ_x reaches R_t, tension failure will occur at the defect in the rock. From the solutions of Eq. (20) and Eq. (21), when the rock is under pressure, the tensile stress $\Delta\sigma_x$ induced by the accumulated stress at the defect has nothing to do with hydrostatic pressure -σ_3. Therefore, Eq. (21) holds as long as the rock is under pressure, whether it is tensionally compressed, uniaxially compressed or triaxially compressed.

Taken together, when local tension failure occurs in a rock under pressure, the maximum principal stress σ_1 is expressed as:

$$\frac{6(R_t+\sigma_3)}{K} = \sigma_1 \quad (\sigma_1 > 0) \quad (22)$$

According to the development process of tension cracks in Figure 2, it is suggested that local macro tension failure occurs inside the rock when the axial force σ_z reaches the uniaxial compressive strength R_c. According to Eq. (16), we have:

$$R_t = \frac{1}{6}KR_c \quad (23)$$

Substituting Eq. (23) into Eq. (22) yields:

$$\frac{R_c}{R_t}\sigma_3 + R_c = \sigma_1 \quad (24)$$

For a rock with defective structures, Eq. (24) can serve as the mechanical condition for local tension failure in this rock when under pressure. Studies have demonstrated that these defects are very small in size. In Figure 2, for example, before the rock is loaded, the internal defect is sized only 2.119 $5\times10^4\mu$m (Zhu et al., 2013). A defect of this size should be objectively existent in most rocks.

3. APPLICABILITY OF THE PRESSURE TENSION STRENGTH CRITERION

Extensive tests have demonstrated that when local tension failure occurs in a rock sample under pressure, the yield strength of this rock is quite low (Yang et al., 2006; Liang et al., 2017). In fact, the strength of a rock block is primarily determined by the bonding force between the minerals and particles that make up the rock and the existence of microcracks; the controlling factors of rock strength are the structural planes in, and the structural features of, the rock (Qian et al., 2010). This suggests that the existence of tension fracture surfaces makes a great difference to

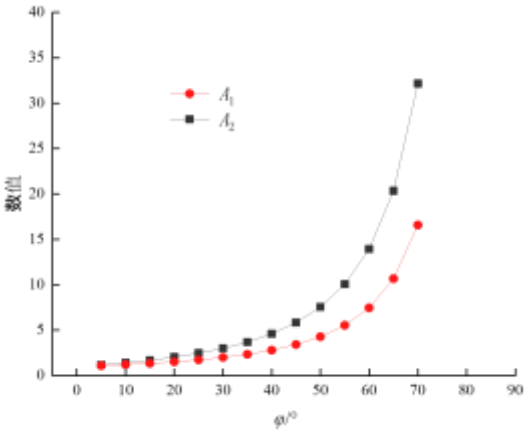

Fig. 4 Changes of A_1 and A_2 with φ.

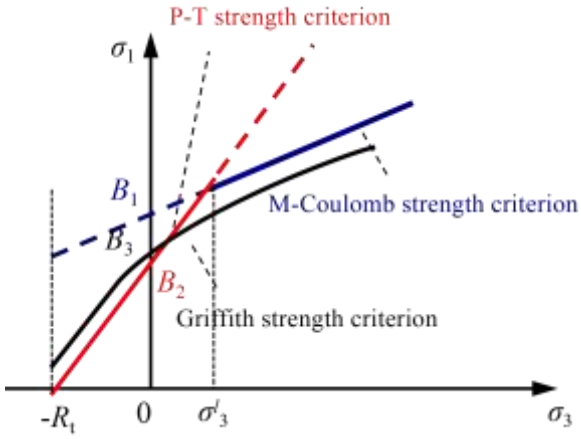

Fig. 5 Comparison of strength criterion curves.

the yield strength of the rock sample. In view of this, we suggest that tension fracture surfaces can be decisive to the yield strength of a rock sample. We also believe that Eq. (22) is the expression of the yield strength of a rock sample under pressure when tension failure occurs. On this basis, a new strength criterion of pressure-tensile (P–T) failure is proposed. Next is a detailed description on the applicability of this strength criterion.

The basic concept of the P–T strength criterion is roughly the same as Griffith strength theory (Qian et al., 2010). Both hold that stress will accumulate at a crack (defect) to cause rock tensile failure. Both can explain why rock tensile failure occurs under P–T state. In this term, the P–T strength criterion concurs with Griffith theory except that it is expressed in a different way. Griffith strength theory emphasizes that rock failure is caused by tension regardless of stress state, but it cannot explain why shear failure occurs under high confining pressure. Rock shear strength is usually estimated by Mohr–Coulomb criterion. Currently, Griffith theory applies only to estimating the strength of brittle rocks, simply because a connection cannot be established between Griffith strength criterion and Mohr–Coulomb criterion. That is, it cannot explain how rock failure changes from tensile to shear with increasing confining pressure. As rocks are complex themselves and their attributes vary, it is very hard to describe rock failure under different stress states with one theory alone.

In this section, the P–T strength criterion, Griffith strength criterion, and Mohr–Coulomb criterion are compared to show the applicability and superiority of the P–T criterion. Assuming that the stress concentration coefficient K at the defect in the rock is immune to σ_3, namely, it is a constant, then Eq. (24) can be seen as the typical expression of the P–T strength criterion. According to the Mohr–Coulomb strength criterion, we have:

$$\frac{1+\sin\phi}{1-\sin\phi}\sigma_3 + \frac{2C\cos\phi}{1-\sin\phi} = \sigma_1 \tag{25}$$

And from Eq. (24) and Eq. (25):

$$A_1 = \frac{1+\sin\phi}{1-\sin\phi},\ B_1 = \frac{2C\cos\phi}{1-\sin\phi},\ A_2 = \frac{R_c}{R_t},\ B_2 = R_c$$

Triaxial compression tests usually involve calculation of C and φ with data points at which pure shear failure occurs in a rock sample over the medium-and-high confining pressure interval. However, when the resulting C and φ are used to regress uniaxial compressive strength, B_1 is commonly larger than the actual uniaxial compressive strength R_c. Therefore we have:

$$B_2 < B_1 \tag{26}$$

Here A_2 is roughly 6–15 (Misa and Nowakowski. 2021); the common rock internal friction angle is roughly 20°–55°. Accordingly, A_1 should be roughly 1.5–4.3. It can be seen that A_2 is always larger than A_1. If the conclusion of the Mohr–Coulomb skew line strength curve is used (Qian et al., 2010) A_2 can be expressed as:

$$A_2 = \frac{R_c}{R_t} = tan^2(45° + \frac{\phi}{2}) \tag{27}$$

From Eq. (25) and Eq. (27), both A_1 and A_2 are relevant to rock internal friction angle φ. Figure 4 shows how A_1 and A_2 change with internal friction angle.

The conclusion that A_2 is always larger than A_1 can be further confirmed by Figure 5, which compares the Mohr–Coulomb strength criterion with the pressure tension strength criterion.

According to Griffith theory, the strength is expressed as:

$$\begin{cases} \sigma_3 = -R_t & (\sigma_1 + 3\sigma_3 < 0) \\ R_t = \frac{(\sigma_1-\sigma_3)^2}{8((\sigma_1+\sigma_3)} & (\sigma_1 + 3\sigma_3 > 0) \end{cases} \tag{28}$$

Figure 5 compares the curves of Mohr–Coulomb strength criterion, Griffith strength criterion, and the P–T strength criterion when $B_3 = 8R_t$.

Between Griffith criterion and Mohr–Coulomb criterion, as $B_3 < B_1$ in general, within $-R_t \le \sigma_3$, the Griffith strength is always smaller than the Mohr–Coulomb strength. That is, the rock is always subject to tensile failure, which is not the case in reality. In fact, under high confining pressure, the actual rock failure strength is closer to Mohr–Coulomb theoretical strength. When $B_3 \ge B_1$, within $\sigma_3 \ge 0$, the Griffith theory strength is always larger than the Mohr–Coulomb theory strength. Hence it cannot explain why rock tensile failure occurs under low confining pressure. Obviously, a connection cannot be established between these two criteria.

Between the P–T criterion and Mohr–Coulomb criterion, when rock is loaded within $-R_t \le \sigma_3 \le \sigma_3^l$, σ_1 first meets the P–T strength criterion, hence tensile failure occurs; after $\sigma_3^l \le \sigma_3$, σ_1 first reaches Mohr–Coulomb criterion, hence shear failure occurs. These facts perfectly explain the objective reality that with the increase of σ_3, rock failure changes from tensile to shear; rock strength is lower than the Mohr–Coulomb theory strength under both P–T state and low confining pressure.

Between the P–T criterion and Griffith criterion, when $\sigma_3=0$, Griffith criterion assumes rock failure strength to be 8 times the R_t, whereas the P–T criterion assumes rock failure strength to be the real measurement of uniaxial compressive strength R_c. In this term, the P–T criterion is more accurate than Griffith criterion. When $B_2 = B_3$, within $-R_t \le \sigma_3 \le 0$, the failure strength values are quite close expect some minor difference in distribution pattern—the Griffith strength curve is parabolic whereas the P–T strength curve is linear. After $\sigma_3 > 0$, especially under high confining pressure, the curves begin to diverge considerably.

As such, using the P–T criterion together with Mohr–Coulomb criterion would give a more realistic picture of rock failure strength and failure characteristics under different stresses. The prerequisite for using the P–T failure criterion to determine rock tensile failure is that the rock is stressed, namely, $\sigma_1 > 0$. Also, from Figure 5, it can be seen that the P–T criterion applies when $-R_t \le \sigma_3 \le \sigma_3^l$.

According to Figure 5, $\sigma^l{}_3$ is defined as the critical confining pressure at which the mode of rock failure changes, then $\sigma^l{}_3$ can be expressed as:

$$\sigma^l{}_3 = \frac{B_1 - B_2}{A_2 - A_1} \tag{28}$$

From Eq. (28), critical confining pressure $\sigma^l{}_3$ is affected by φ, R_c, R_t *and* C, with C and φ being the stabilizing C and φ over the medium-and-high confining pressure interval in triaxial compression tests.

4. FAILURE CHARACTERISTICS UNDER THE P–T STRENGTH CRITERION

4.1. FAILURE CHARACTERISTICS AT THE TIME OF LOADING UNDER THE P–T STRENGTH CRITERION

Within $-R_t \le \sigma_3 \le \sigma^l{}_3$, the resultant force σ_x of rock tension failure is the superimposition of the tensile stress $\Delta\sigma_x$ of the accumulated stress at the defect in the compressed rock in the horizontal direction with the hydrostatic pressure σ_3. The hydrostatic pressure σ_3 is well directional while the accumulated stress is decomposable in other directions. As a result, within $-Rt \le \sigma_3 \le \sigma^l{}_3$, the larger the proportion of σ_3 is in σ_x, the more parallel the rock tension fracture surface is to the direction of σ_1, and accordingly, the greater the tension failure is on the fracture surface.

In fact, there are generally many defects in rock samples. These defects are anisotropic. Stress concentration coefficient K and defect size s differ from one defect to another. When the rock sample is compressed within $-R_t \le \sigma_3 \le \sigma^l{}_3$, the uneven stressing on different defects also tends to result in different failure modes. This combination of tension and shear failure tends to assimilate with the increase or reduction of σ_3.

4.2. FAILURE CHARACTERISTICS AT THE TIME OF UNLOADING UNDER THE PRESSURE TENSION STRENGTH CRITERION

Assuming that the rock is triaxially compressed with its stress state at point H ($R_c < \sigma_1 < \frac{R_c}{R_t}\sigma_3{}^l + R_C$), where the rock has yet to reach the mechanical condition for any shear or tension, as shown in Figure 6(a), when the minimum principal stress σ_3 is suddenly unloaded, the stress state of the rock will tend toward the pressure tension failure strength curve. Local tension failure parallel to the direction of σ_1 will appear inside the rock. One common manifestation of such failure is splitting failure on the surrounding rock surface after roadway excavation.

Assuming that the stress state at point H satisfies $R_C < \sigma_3 < \frac{R_c}{R_t}\sigma_z{}^l + R_C$, as shown in Figure 6(b), where the rock still doesn't reach the mechanical condition for any shear or tension, when the maximum principal stress σ_1 is suddenly unloaded, σ_3 becomes the maximum principal stress. In that case the stress state of the rock will again tend toward the pressure tension failure strength curve, but the direction of its tension cracks will change. One common manifestation of such failure is the diametrical cracking of borehole cores in deep underground works.

5. ACCURACY VERIFICATION OF THE PRESSURE TENSION STRENGTH CRITERION

Throughout the history of rock mechanics, each classic strength theory or criterion has been verified by numerous researchers through extensive field practice and laboratory tests. Hence related research and laboratory test results are referenced to verify the universality and accuracy of the pressure tension strength criterion.

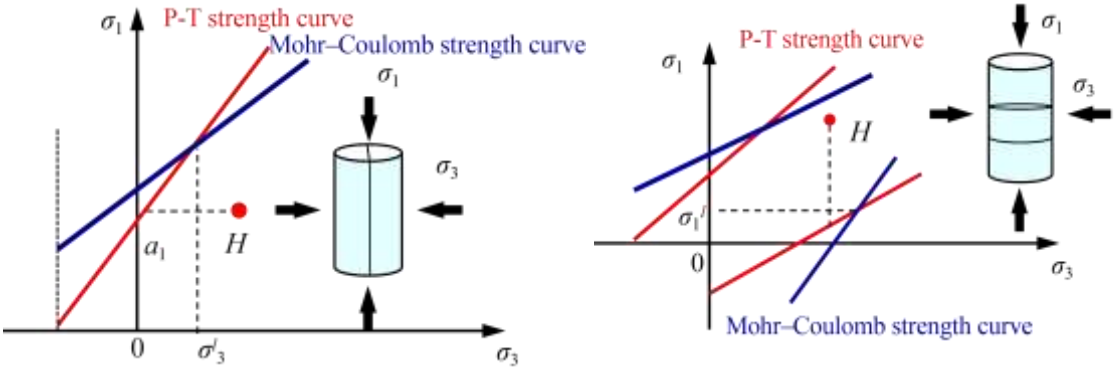

(a) Failure when σ_3 is unloaded (b) Failure when σ_1 is unloaded

Fig. 6 Failure characteristics of rock under different unloading conditions.

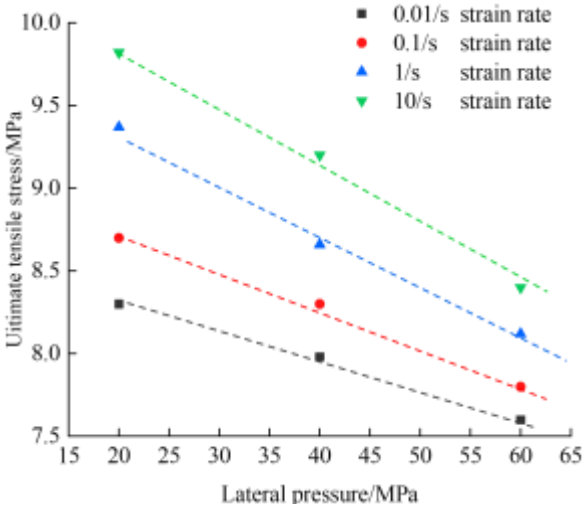

Fig. 7 Relationship between lateral pressure and tensile strength (Yuan, 2013).

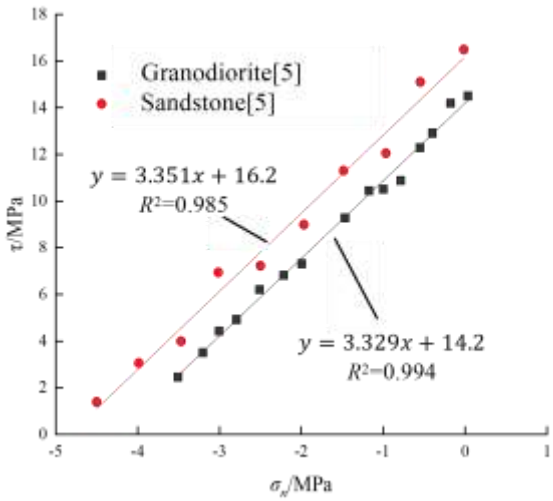

Fig. 8 Scatter diagram of shear stress and tensile stress of granite and marble under tension shear failure (Li et al., 2014).

5.1. THEORY VERIFICATION

To verify the reliability of the pressure tension failure strength criterion, the first thing to do is to verify its theory. According to the derivation process described in chapter 2, it is suggested that a tensile stress perpendicular to the direction of the compressive stress will be produced at the defect inside a rock sample under pressure, as expressed by Eq. (20); there will be a linearity between the tensile stress produced at the defect and the compressive stress. Yuan (2013) presented the result of a direct tensile test conducted on granite, as shown in Figure 7.

From Figure 7, under the same strain rate, as the lateral pressure increases, the ultimate tensile stress for the granite reduces linearly. If this phenomenon were to be explained with the pressure tension strength theory, then as the lateral pressure increases, the tensile stress produced at the defect inside the granite grows linearly. The sum of this tensile stress and the ultimate tensile stress for the exterior of granite is the uniaxial tensile strength R_t. Again from this diagram, there is indeed a linearity between the amount of increase of lateral pressure and the amount of reduction of the ultimate tensile stress for granite. The pressure tension strength theory well explains the test result. A similar result has also been reported by Liu (2007), who conducted the same tests on gypsum and granite. This further confirms that the P–T strength theory has scientific grounds.

5.2. STRENGTH VERIFICATION

According to the foregoing analysis, the P–T strength criterion applies to low shear stressing. According to the test data we have collected, by test type, low shear stressing can include tension-shear tests, pressure-shear tests and low confining-pressure triaxial compression tests.

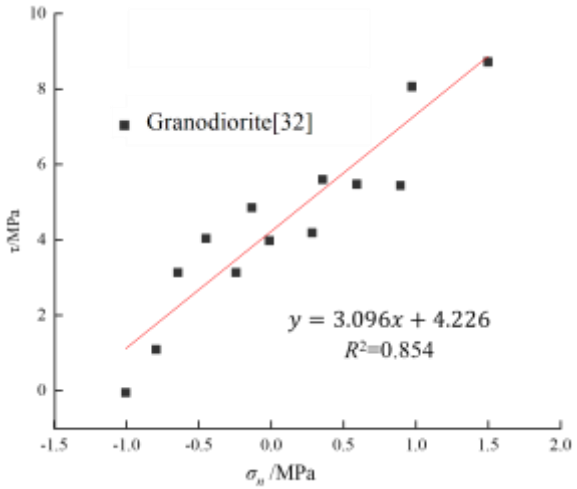

Fig. 9 Scatter diagram of shear stress and tensile stress of diorite granite under tensile shear failure.

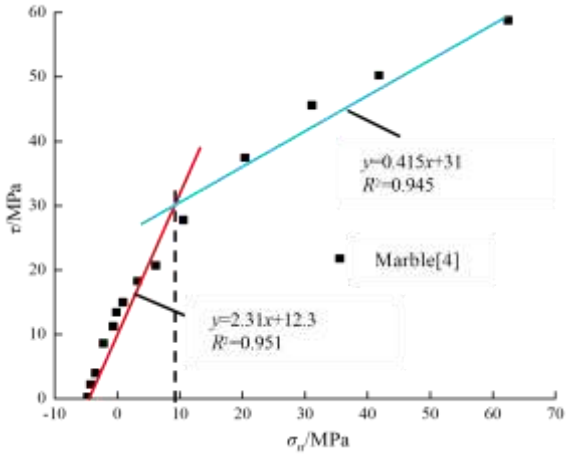

Fig. 10 Scatter diagram of shear stress and tensile stress of marble under tensile shear failure.

1. Tension-shear tests

Tension shear tests give a more intuitive picture of the strength of rock samples under low shear stresses. Figure 8 shows the result of tension shear tests on granite and sandstone in Li et al. (2014). When the rock sample is tensioned and sheared, there is a detectable linearity between its shear stress and tensile stress. Assuming that in a tension shear state, the relationship between shear stress and tensile stress is:

$$\tau = D\sigma_n + E \tag{29}$$

where: τ—shear stress, MPa;

σ_n—normal stress, MPa; D and E are constants.

According to elastic mechanics, the relationship between principal stress and tensile/shear stress is:

$$\begin{cases} \sigma_n = \frac{\sigma_1+\sigma_3}{2} + \frac{\sigma_1-\sigma_3}{2}\cos 2\theta \\ \tau = \frac{\sigma_1-\sigma_3}{2} sin\, 2\,\theta \end{cases} \tag{30}$$

Here, θ—angle between the principal axis direction and the rupture surface, °. As noted by reference (Li et al., 2014) in a tension shear test, almost all rock failures occur along a given shear surface. Hence in these tests, θ can be seen as a fixed constant. By substituting Eq. (29) into Eq. (30), the relationship between principal stresses can be obtained:

$$\frac{G}{F}\sigma_3 - \frac{2E}{F} = \sigma_1 \tag{31}$$

where: $F = D - D\cos 2\theta - sin\, 2\,\theta,$

$G = D\cos 2\theta - D - sin\, 2\,\theta.$

From Eq. (31), there is also a linear connection between maximum and minimum principal stresses. According to the boundary conditions, when σ3=0, σ1=Rc; when σ1=0, σ3=Rt. In that case, the slope of the skew line strength curve is Rc/Rt. This derives the strength relationship of a rock sample under tension and pressure as:

$$\frac{R_c}{R_t}\sigma_3 + R_C = \sigma_1 \tag{32}$$

From the analysis above, in a tension shear test, if there is a linearity between shear stress and tensile stress, the P–T strength criterion is definitely satisfied.

2. Tension-shear and pressure-shear tests

Figure 9 shows the relationship between shear stress and normal stress obtained by Zhou et al. (2016) from tension-shear and pressure-shear tests on granodiorite.

At -1 MPa≤σ_n≤1.5 MPa, all rock failure surfaces show features of tension failure [32]. By fitting with the result in Figure 10, when -1 MPa≤σ_n≤1.5 MPa, shear stress increases with the increase of normal stress. This strong linearity indicates that the tension shear and pressure-shear test data also satisfy the P–T strength criterion.

Figure 11 shows the relationship between shear stress and normal stress σ_n obtained by Zhou et al. (2014). from tension-shear and pressure-shear tests on marble.

As shown in Figure 10, reference Zhou et al. (2016) noted that within -5 MPa≤σ_n＜10 MPa, rock fracture surface shows obvious signs of tensile failure; after σ_n≥10 MPa, pure shear failure occurs in the rock sample. Hence according to the difference in failure form, data at -5 MPa≤σ_n＜10 MPa and σ_n≥10 MPa are fitted into two strength curves. The high correlation coefficient between both failure strength curves with the test data indicates an internal connection between failure form and failure strength. Both strength curves show a high linear relationship and can be regarded as a P–T strength curve and a shear strength curve. This further confirms that using the P–T strength criterion together with Mohr–Coulomb criterion can give more accurate description of rock strength under different stress states.

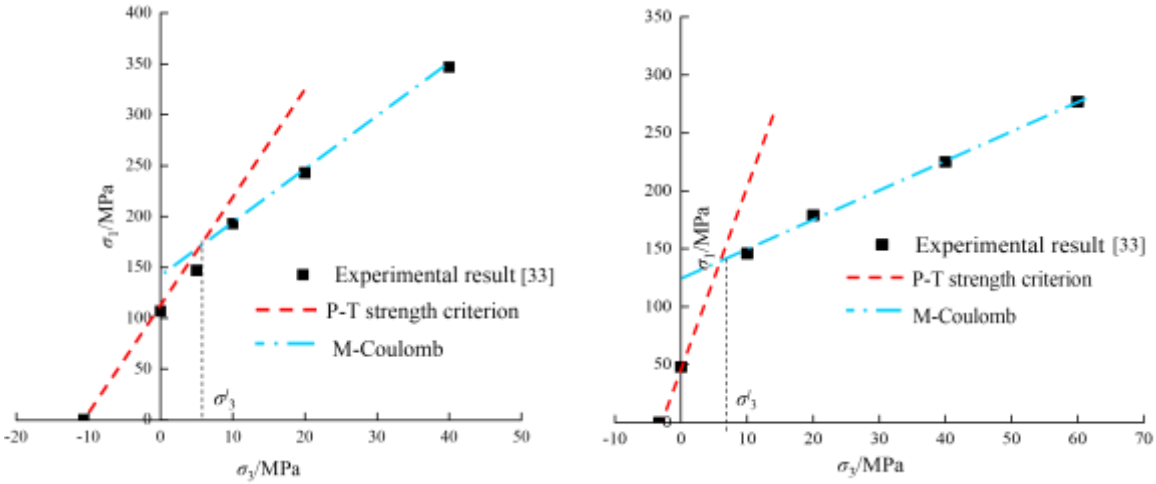

(a) Hornstone (b) marble

Fig. 11 Rock strength evolution in triaxial compression tests.

3. *Triaxial compression tests*

Figure 11 shows the strength parameters and triaxial compression test results of hornstone and marble reported by Zhang and Liu (2016).

From these diagrams, the change of yield strength for both hornstone and marble in the test takes place at σ_3=10 MPa. According to the R_c and R_t values provided by the reference, for both rocks, the intersection between the Mohr–Coulomb criterion strength curve and the P–T strength curve is located before the inflection; before the inflection, the yield strength of both rocks more approximates the P–T strength curve. This suggests that in these triaxial compression tests, it is more appropriate to characterize the yield strength of a rock sample before the inflection of the critical confining pressure σ^l_3 with the P–T strength criterion.

From Figure 11, the inflection point of both hornstone and marble falls at σ_3=10 MPa. Their critical confining pressure σ^l_3 both lies before the inflection point. Before the inflection point, the yield strength of both rock samples is closer to the P–T strength curve. After the inflection point, it is closer to the Mohr–Coulomb curve. Hence in the triaxial compressive test above, it is more appropriate to use the P–T criterion together with Mohr–Coulomb curve to characterize the yield strength of rock samples.

5.3. *VERIFICATION OF THE CRITICAL CONFINING PRESSURE*

Previous studies have demonstrated that triaxial compression tests are mostly focused on high confining pressures (Liu et al., 2014; Wang et al., 2010; Wang et al., 2012; Yang et al., 2006). Also, as the σ^l_3 of some rocks is relatively small, the availability of test data for low confining pressures smaller than σ^l_3 is quite limited. If we tried to verify the accuracy of the P–T strength criterion by summarizing the linearity between test data points for low confining pressures from axial compression tests, the conclusion would not be so persuasive. Hence the theory calculation result of critical confining pressure σ^l_3 is compared with the confining pressure interval in which the failure mode changes as expressly noted by the related references to further investigate the reliability of the calculated critical confining pressure σ^l_3 and verify the accuracy of the P–T strength criterion.

In order to further validate the calculated critical confining pressure σ^l_3, five sets of test results are summarized from existing references and compared with the theory calculation result of critical confining pressure σ^l_3, as shown in Table 1. It should be noted that as none of the references include any tensile strength test result, R_t is assumed to be R_c/6 and R_c/15 (Misa et al., 2021). To facilitate expression, σ^k_3 is

Table 1 Test data statistics and analysis.

Lithology	C/ MPa	φ_p	R_c/ MPa	σ^k_3/ MPa	σ^l_3/ MPa (R_t=R_c/6)	σ^l_3/ MPa (R_t=R_c/15)	Source of data
Coal	11.6	23.5	17.7	0–10	4.8	1.4	Su et al., 2006
Coal	12.7	24.1	22.5	0–10	4.6	1.3	Liu et al., 2014
Coal	12.1	33.6	30.1	0–8	6	1.3	Liu et al., 2014
Sandstone	16.3	32.6	46.5	0–5	4.8	1.1	Niu, 2011
Marble	42.5	28.4	93	0–20	15.5	4	Zhang et al., 2010

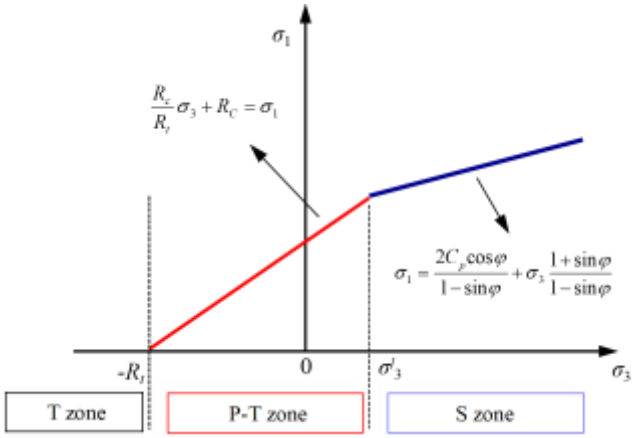

Fig. 12 Element yield criterion in the model.

used to represent the interval of confining pressure σ_3 in which the mode of rock failure in the tests changes from a failure with tension features to pure shear failure.

From Table 1, at R_t=R_c/6–R_c/15, the theory calculation result of critical confining pressure σ^J_3 for all rocks except shale is within the interval of σ^k_3. For shale, when the compressive strength R_t is within R_c/9–R_c/14, the calculated σ^J_3 also agrees with the test result. This suggests that the calculation method for critical confining pressure σ^J_3 is quite appropriate. It also confirms the accuracy of the P–T strength criterion.

To sum up, we have tried to analyze the strength of rocks under low shear stresses from different perspectives, using 5 kinds of rocks with different lithologies, three different test methods and multiple sets of test data. The result further verifies the universality and accuracy of the P–T strength criterion.

6. COMPARISON WITH THE TRADITIONAL PLASTIC ZONE CRITERION

The P–T strength criterion can predict surrounding rock plastic zones in underground roadways, evaluate surrounding rock stability and provide theoretical basis for designing the support of roadway surrounding rock. In this section, FLAC3D is used to compare surrounding rock plastic zone distribution before and after P–T strength criterion is incorporated in rock failure analysis.

6.1. MODEL BUILDING

In the previous section, we have verified the accuracy of the P–T strength criterion, which broadens the way of investigating roadway surrounding rock failure and evaluating the stability of underground works and provides theory basis for designing supports for roadway surrounding rock.

According to the three strength criteria and the rock stress environment, plastic failure zones can be categorized as tensile failure zones (T zones), pressure-tensile failure zones (P–T zones), and share failure zones (S zones). Here a T zone is an area where tensile failure occurs under tensile stress alone. A P–T zone its an area where tensile failure occurs under compressive stress or under both tensile and compressive stresses. Figure 12 compares the yield criteria among different failure zones. The equations in the diagram are rewritten as an inequality and used as the criteria for discriminating between tensile failure, pressure–tensile failure, and shear failure.

$$-R_t \geq \sigma_3 \tag{33}$$

$$\frac{R_C}{R_t}\sigma_3 + R_C < \sigma_1 \tag{34}$$

$$\frac{2C\cos\phi}{1-\sin\phi} + \frac{1+\sin\phi}{1-\sin\phi}\sigma_3 \leq \sigma_1 \tag{35}$$

where: C—initial cohesion, MPa;

To ensure that the P–T strength criterion applies well to field engineering practices, based on FLAC3D, a model (PT–PS model) capable of identifying T zones, P–T zones and S zones is built. Eqs. (33) – (35) are embedded into the simulated FLAC3D model by writing FISH language. The determination process is as shown in Figure 13. It is also assumed that throughout the calculation, any tension failure in the surrounding rock will not affect its strength parameters (C, φ). This way, the T zones, P–T zones and S zones are identified only according to the stress state of the surrounding rock.

A numerical model geometrically sized x×y×z=100 m×10 m×100 m is built. The model is equally gridded at the size of 0.5 m. At the center of the model is a 3×3 m rectangular roadway. The entire bottom surface of the model is fixed. Uniform load is applied on both the upper surface and the sides. Figure 14 shows the stressing of the model, where σ_x=σ_y. The model is a Mohr-Coulomb constitutive model. To simplify calculation, the surrounding rock is comprised of one single lithology (argillaceous sandstone). The base parameters of roadway surrounding rock are as follows: σ_x=σ_y=30MPa, elastic modulus E=10 GPa, Poisson's ratio v=0.28, cohesion

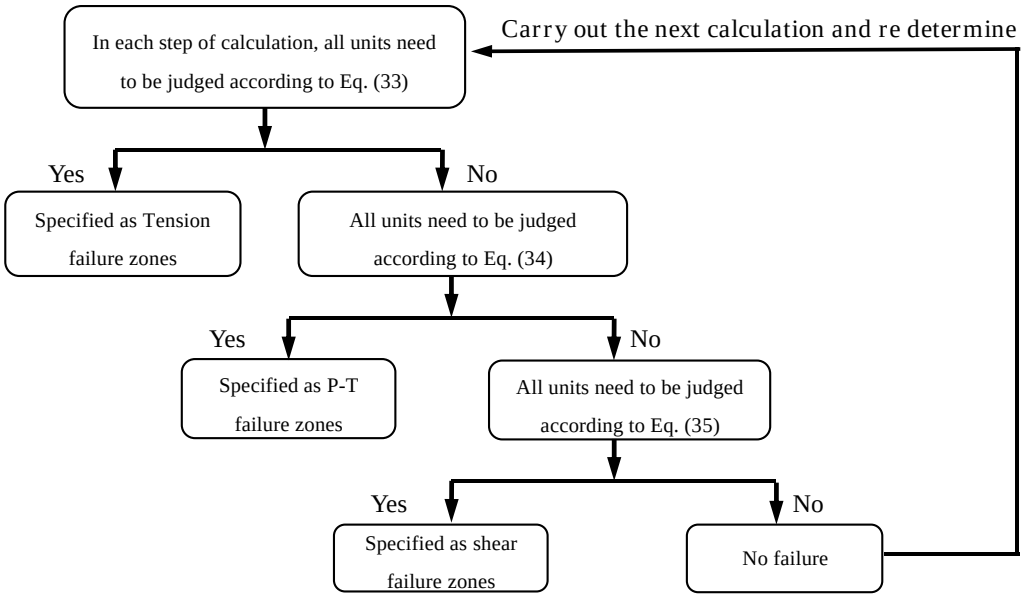

Fig. 13 Determination proces.

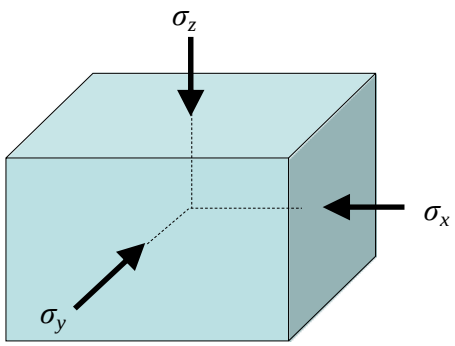

Fig. 14 Model stressing diagram.

C=10MPa, uniaxial tensile strength R_t=3.6 MPa, uniaxial compressive strength R_C=25 MPa, and internal friction angle φ=30°.

6.2. COMPARISON

In underground works, many roadways are affected by face mining, resulting in noticeable changes in the stress field around the surrounding rock. In the numerical model, σ_x=σ_y=30 MPa is defined as a constant value. Roadway surrounding rock stress is changed by changing the value of σ_z. Figure 15 compares the surrounding rock plastic zone distribution between the traditional model and the PT–PS model when the confining pressure coefficient λ=1 (σ_z=30 MPa).

As shown in Figure 15, the plastic zones in the two models are the same except for the mode of surrounding rock failure. The traditional model considers that only shear failure occurs on the roadway side, as shown in Figure 15(a), whereas in the PT–PS model, from the roadway wall to the interior of the surrounding rock, the mode of rock failure in the plastic zone changes from tensile to shear, as shown in Figure 15(b). In fact, after roadway excavation, the boundary stress is released. The roadway surface surrounding rock is under a low confining pressure, which gradually rises from the roadway wall to the interior. Tension failure in roadway surface surrounding rock and shear failure in deep surrounding rock seems to be more common. Zhang et al. (2010) discovered through observation of deep underground caverns that from the cavern wall down to the depth, the mode of marble failure changes from axial splitting failure to inclined single-crack shear

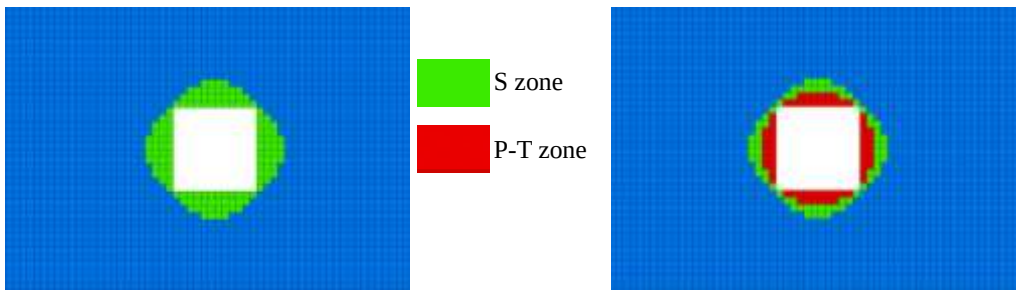

(a) Traditional model (b) PT–PS model

Fig. 15 Plastic zone distributions in different models when λ=1.

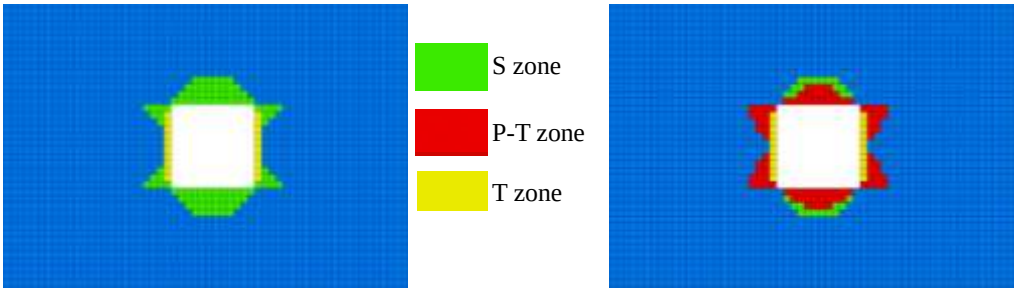

(a) Traditional model (b) PT–PS model

Fig. 16 Plastic zone distributions in different models when λ=3.

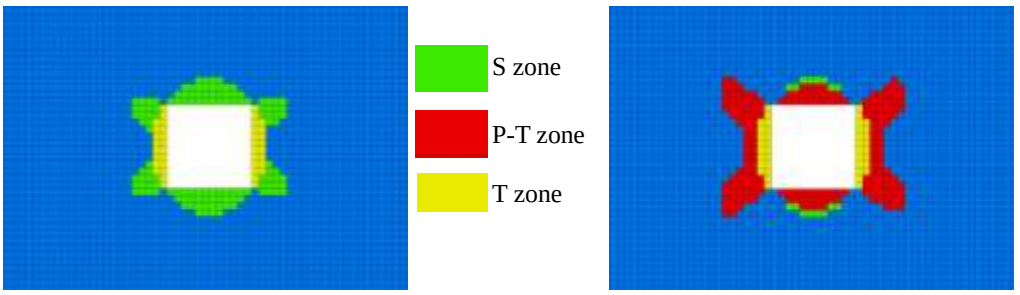

(a) Traditional model (b) PT–PS model

Fig. 17 Plastic zone distributions in different models when λ=6.

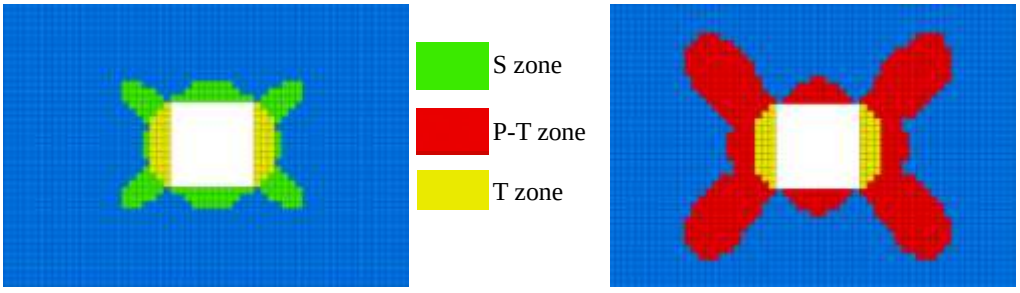

(a) Traditional model (b) PT–PS model

Fig. 18 Plastic zone distributions in different models when λ=9.

failure. Dai (2007) yielded the same result when observing mining roadway failure in 1304 face of Xinglongzhuang coal mine. Both examples verify that the PT–PS criterion determines the surrounding rock failure form more accurately.

Studies have revealed existence of obvious tensile stress zones in the roadway surrounding rock when $\lambda \leq 1/3$ and $\lambda \geq 3$[29]. Considering that the main function of the P–T strength criterion is to identify rock failure strength under P–T state, to better clarify the difference between the traditional model and the PT–PS model in identifying surrounding rock plastic zone, the plastic zone distributions at λ = 3, 6, 9 (σz=10 MPa, 5 MPa, 2.5 MPa) are calculated for both models, as shown in Figures 16–18.

As illustrated, under the same conditions, the plastic zones in the two models are the same in roof and floor except for the form of surrounding rock failure. After $\lambda \geq 3$, tensile stress occurs in the roadway sidewalls, giving rise to T zones, which gradually enlarge with increasing λ. Also, under the same conditions, the range of the T zones is the same for the two models, too. In the roadway sidewalls, as the depth increases, the surrounding rock stress changes from tensile, compressive tensile to compressive. As the traditional model overestimates the rock strength under P–T state, the range of the surrounding rock plastic zones determined by PT–PS model is larger than by the traditional model. After $\lambda \geq 3$, as λ further increases, more surrounding rock in the roadway sidewalls is under P–T state, adding to the difference between the two calculations.

7. CONCLUSIONS

1. Based on the hypothesis of a nonuniform rigid body mode, the equation describing the tensile stress induced by the accumulated stress at the defect in a rock under uniaxial or hydrostatic

pressure is deduced. In the light of the theory of maximum normal stress, the formation mechanism of tension cracks in rocks under pressure is revealed. A P–T strength criterion is proposed.

2. The relationship between the P–T strength criterion and Mohr–Coulomb strength criterion is established. The applicable range of the P–T strength criterion is identified as-$R_t \leq \sigma_3 \leq \sigma^l_3$. The P–T strength criterion is compared with the Mohr–Coulomb strength criterion. The applicable range of the new strength criterion is identified as -$R_t \leq \sigma_3 \leq \sigma^l_3$. The objective realities that under low confining pressures the rock failure strength is lower than the triaxial linear regression strength and the rock failure mode changes from tension to shear with the increase of confining pressure are explained. By summarizing related test results, the universality and accuracy of the P–T strength criterion are verified.
3. A PT–PS model capable of identifying P–T zones is built and compared with the traditional model. As the traditional model overestimates rock strength under P–T state, after $\lambda \leq 1/3$ and $\lambda \geq 3$, the traditional model underestimates the range of the roadway surrounding rock plastic zone. This underestimation will further increase as λ decreases ($\lambda \leq 1/3$) or increases ($\lambda \geq 3$).
4. The PT–PS model gives a more realistic picture of roadway surrounding rock failure. The PT–PS model can provide meaningful reference for evaluating the stability and designing the supports of underground works.

DATA AVAILABILITY

The data used to support the findings of this study are available from the corresponding author upon request.

CONFLICTS OF INTEREST

On behalf of all authors, the corresponding author states that there is no conflict of interest.

REFERENCES

Alejano, L.R., Arzua, J., Bozorgzadeh, N. and Harrison, J.P.: 2017, Triaxial strength and deformability of intact and increasingly jointed granite sample. Int. J. Rock Mech. Min. Sci,, 95, 87–103. DOI: 10.1016/j.ijrmms.2017.03.009

Arzua, J. and Alejano, L.R.: 2013, Dilation in granite during servo-controlled triaxial strength tests. International Int. J. Rock Mech. Min. Sci.,, 61, 43–56. DOI: 10.1016/j.ijrmms.2013.02.007

Arzua, J., Alejano, L.R. and Walton, G.: 2014, Strength and dilation of jointed granite specimens in servo-controlled triaxial tests. Int. J. Rock Mech. Min. Sci.,, 69, 93–104. DOI: 10.1016/j.ijrmms.2014.04.001

Cen, D.F., Liu, C. and Huang, D.: 2020, Experimental and numerical study on tensile-shear strength and rupture characteristics of sandstone. Chinese Journal of Rock Mechanics and Engineering, 39, 07, 1333–1342, (in Chinese). DOI: 10.13722/j.cnki.jrme.2019.1093

Dai, J.: 2007, Crack propagation and slab like structure of surrounding rock of fully mechanized top coal caving roadway and its non-uniform control. Ph.D. thesis, Shandong, University of Science and Technology, Qingdao, China.

Denise, D, and Quevedo, F.: 2020, Analytical solution of deep tunnels in a strain-hardening elasto-plastic rock mass. Lat. Am. J. Solids Struct,, 17, (6), e297. DOI: 10.1590/1679-78256023

Guo, J.Y., Li, X., Li, S.D., Hao, J.M., Yuan, W.N., Dong, G.F. and Wang, Y.S.: 2012, The engineering geology mechanical properties of rock in tension-shear state. J. Eng. Geol.,, 20 (06), 1020–1027.

Huang, D., Li, Y. and Cen, D.F.: 2020, Strength and Failure of mechanism of brittle rocks under tensile-compressive ressive stress state with partical flow simulation. J. Eng. Geol., 28 (04), 677–684. DOI: 10.13544/j.cnki.jeg.2019-339

Huang, F., Li, T.Y., Gao, X.Y., Yang, X. and Lin, Z.: 2019, Study on the macro-micro failure mechanism of granite and its geometry effect under the different conditions of confining pressure by discrete element. J. China Coal Soc., 44 (03), 924–933, (in Chinese). DOI: 10.13225/j.cnki.jccs.2018.0070

Jiang, H.K., Zhang, L. and Zhou, Y.S.: 2000, Behavior of acoustic emission time sequence of granite in deformation and failure process under different confining pressures. Chin. J. Geophys., 43, 06, 812–826, (in Chinese).

Li, G., Ma. F.S., Guo, J., Zhao, H.J. and Liu, G.: 2020, Study on deformation failure mechanism and support technology of deep soft rock roadway. Eng. Geol., 264, Article ID 7475698. DOI: 10.1016/j.enggeo.2019.105262

Li, S.D., Li, X., Guo, J.Y., Hao, J.M. and Liu, Y.H.: 2014, Research of rock failure testing under combined shear and tension. J. Eng. Geol., 22 (4), 655–666. DOI: 10.13544/j.cnki.jeg.2014.04.011

Liang, Y.P., Li, Q.M., Gu, Y.L., Zhou, Q.L. and Li, Q.G.: 2017, Experimental study on characteristics of post-peak residual strength and fracture surface of shale under various confining pressures. Journal of Mining & Safety Engineering, 34 (06), 1179–1185, (in Chinese). DOI: 10.13545/j.cnki.jmse.2017.06.022

Liu, Q.S., Liu, K.D. and Zhu, J.B.: 2014, Study of mechanical properties of raw coal under high stress with triaxial comperession. Chin. J. Rock Mech. Eng., 33, 01, 24–34, (in Chinese). DOI: 10.13722/j.cnki.jrme.2014.s2.006

Liu, S.Q.: 2007, Studies on dynamic tensile properties of granite under confining pressure. Ph.D. thesis, Graduate University of Chinese Academy of Sciences, Wuhan, China.

Misa, R. AND Nowakowski, A.: 2021, Comparison of the Compressive and Tensile Strength Values of Rocks Obtained on the Basis of Various Standards and Recommendations. Symmetry, 13, 7, 1163. DOI: 10.3390/SYM13071163

Niu, S.J.: 2011, Study on Strength Degradation Law of Surrounding Rock of Deep Roadways. Ph.D. thesis, China University of mining and technology, Xuzhou, China.

Qian, M.G., Shi, P.W. and Xu, J.L.: 2010, Mining Pressure and Strata Control. Xuzhou, China, China University of mining and Technology, Press.

Ramsey, J.M. and Chester, F.M.: 2004, Hybrid fracture and the transition from extension fracture to shear fracture. Nature, 428 (6978), 63–66. DOI: 10.1038/nature02333

Ramsey, J.M.: 2003, Experimental study of the transition from brittle shear fractures to joints. Ph.D. thesis, Texas A & M University, Texas, USA.

Ren, F.: 2018, Mechanical Properties and Failure Modes of Coal and Rock Under Triaxial Compression. Safety in Coal Mines, 49 (01), 37–39, 43, (in Chinese). DOI: 10.13347/j.cnki.mkaq.2018.01.010

Rodionov, V.N., Sizov, I.A. and Tsvetkov, V.M.: 1986, Fundamentals of geomechanics. Moscow: Nedra, (in ussian).

Rodionov, V.N. and Sizov, I.A.: 1982, Model of a rigid body with dissipasive structure for geomechanics. J. Min. Sci., 18 (6), 323–331. DOI: 10.1007/BF02498606

Rodriguez, E.: 2005, A micro structural study of the extension-to-shear fracture transition in Carrara marble. Ph.D. thesis, Texas A & M University, Texas, USA.

Su, C.D., Zhai, X.X., Li, Y.M., Li, S.M. and Liu, Z.Y.: 2006, Study on deformation and strength of coal samples in triaxial compression. Chin. J. Rock Mech. Eng., 25, 2963–2968. (in Chinese).

Wang, D., Liu, C.W., Wang, D., Li, X.D. and Xu, Y.H.: 2012, Research on the Tension-shear Deformation and Failure Criterion of Rock Under Complex Stress. J. Sichuan Univ., 44 (2), 31–35, (in Chinese). DOI: 10.15961/j.jsuese.2012.02.003

Wang, D., Han, X.G. and Zhou, X.G.: 2010, Limestone failure law and post-failure constitutive relation in the control of lateral deformation. Journal of coal industry, 35(12), 2022–2027, (in Chinese). DOI: 10.13225/j.cnki.jccs.2010.12.030

Xie, H.P., Gao, M.Z., Fu, C.X., Lu, Y.Q., Yang, M.Q., Hu, J.J. and Yang, B.G.: 2021, Study on mechanical behavior of brittle ductile transformation of rocks at different depths. J. China Coal Soc, 46 (03), 701–715, (in Chinese). DOI: 10.13225/j.cnki.jccs.yt21.0157

Yang, Y.J., Song, Y. and Chen, S.J.: 2006, Test study of coal's strength and deformation characteristics under triaxial compression, J. China Coal Soc., 2, 150–153, (in Chinese).

Yu, Q.L., Yang, T.H., Liu, H.L. and Tang, C.A.: 2009, Numerical simulation on granite failure mechanism at meso-level under moderate or low confining pressure. J. Northeast. Univ., 30(07), 1026–1029, (in Chinese). DOI: 10.3969/j.issn.1005-3026.2009.07.027

Yuan, C.: 2013, The experiment of dynamic direct tensile test for rock under lateral pressure and dynamic fracture mechanics study. Ph.D. thesis, Hunan University of Science and Technology, Xiangtan, China.

Zang, C.W., Chen, M., Zhang, G.C., Wang, K. and, Gu, D,D,: 2020, Research on the failure process and stability control technology in a deep roadway: Numerical simulation and field test. Energy Sci. Eng., 8, 7, 2297–2310. DOI: 10.1002/ese3.664

Zhang, C.Q., Feng, X.T., Zhou, H., Zhang, C.S. and Wu, S.Y.: 2010, Brittle failure of surrounding rock mass in deeo test tunnels and its numerical simulation. Chinese Journal of Rock Mechanics and Engineering, 29(10), 2063–2068.

Zhang, L. and Liu, B.G.: 2016, A comparison study of rock strength criteria. Eng. Mech., 33(11), 201–207, (in Chinese). DOI: 10.6052/j.issn.1000-4750.2015.08.0642

Zhou, H., Lu, J.J., Xu, R.C., Zhang, C.Q., Chen, J. and Meng, F.Z.: 2016, Research on tension-shear failure characteristics and yield criterion of hard brittle marble. Rock Soil Mech., 37, 2, 305–314, 349. DOI: 10.16285/j.rsm.2016.02.001

Zhou, H.M., Xiong, S.H., Liu, X.H., Yang, Z.H. and Kong, X.H.: 2005, In-situ tension-shear tests and strength criterion studies. Chin. J. Rock Mech. Eng., 24, 24, 4418–4421. DOI: 10.1007/s11769-005-0030-x

Zhou, J.W., Xu, W.Y. and Yang, G.: 2010, A microcrack damage model for brittle rocks under uniaxial compression. Mech. Res. Commun., 37, 04, 399–405. DOI: 10.1016/j.mechrescom.2010.05.001

Zhu, Z.D., Huang, Q., Wang, J.B., Shao, J.F. and Wang, W.: 2013, Mesoscopic experiment on degeradation evolution of rock deformation and its meso-dama mechanical model. Chin. J. Rock Mech. Eng., 32, 6, 1167–1175.